General Disclaimer

One or more of the Following Statements may affect this Document

- This document has been reproduced from the best copy furnished by the organizational source. It is being released in the interest of making available as much information as possible.

- This document may contain data, which exceeds the sheet parameters. It was furnished in this condition by the organizational source and is the best copy available.

- This document may contain tone-on-tone or color graphs, charts and/or pictures, which have been reproduced in black and white.

- This document is paginated as submitted by the original source.

- Portions of this document are not fully legible due to the historical nature of some of the material. However, it is the best reproduction available from the original submission.

X-941-77-168
PREPRINT

VISIBLE AND INFRARED IMAGING RADIOMETERS FOR OCEAN OBSERVATIONS

W. L. BARNES

JULY 1977

GODDARD SPACE FLIGHT CENTER
GREENBELT, MARYLAND

X-941-77-168
Preprint

VISIBLE AND INFRARED IMAGING RADIOMETERS FOR OCEAN OBSERVATIONS

W. L. Barnes

July 1977

GODDARD SPACE FLIGHT CENTER
Greenbelt, Maryland

PREFACE

The following paper is part of the Advisory Group for Aerospace Research and Development (AGARD) Lecture Series No. 88 "Application of Remote Sensing to Ocean Surveillance" and will be presented during the period 2-11 October, 1977 in Oslo, Norway; Den Helder, Netherlands; and Rome, Italy.

VISIBLE AND INFRARED IMAGING RADIOMETERS FOR OCEAN OBSERVATIONS

W. L. Barnes

ABSTRACT

This paper deals with the current status of visible and infrared sensors designed for the remote monitoring of the oceans. Emphasis is placed on multichannel scanning radiometers that are either operational or under development. Present design practices and parameter constraints are discussed. Airborne sensor systems examined include the Ocean Color Scanner (OCS) and the Ocean Temperature Scanner (OTS). The Costal Zone Color Scanner (CZCS) and Advanced Very High Resolution Radiometer (AVHRR), upcoming spaceborne sensors for oceanic applications, are reviewed with emphasis on design specifications, expected completion, and anticipated performance. Finally, recent technological advances and their probable impact on sensor design are examined.

CONTENTS

ILLUSTRATIONS

ILLUSTRATIONS (Continued)

TABLES

VISIBLE AND INFRARED IMAGING RADIOMETERS FOR OCEAN OBSERVATIONS

I. INTRODUCTION

The development of imaging radiometers for the purpose of observing a wide variety of surface and atmospheric parameters from airborne or spaceborne platforms has been a rather recent phenomena, occurring almost completely within the last twenty-five years. The application of this technology to oceanography is even more recent with the first imaging visible and infrared radiometer dedicated to oceanography scheduled for launch during the upcoming year (1978).

Imaging the earth's surface was limited to airborne photography until the availability of infrared detectors with short time constants led to the development of thermal strip mappers in the early 1950's. The sensors used a single detector and a scanning mirror with the motion of the aircraft relative to the ground supplying the vertical scan motion. This technology developed rapidly and in November, 1960, the Medium Resolution Infrared Radiometer (MRIR) aboard TIROS II provided the first thermal images of the earth from a space platform. The primary interest in this data was meteorological. Applications to oceanography were minimal due to the 20 n. mi. spatial resolution. It was not until the data from the High Resolution Infrared Radiometer (HRIR) on NIMBUS I became available in 1964 that any meaningful study of the oceans was possible using data from space.

In the interim there has been a considerable research effort to determine which parameters of interest to the oceanographic community are discernable from aircraft or space platforms using visible and infrared radiometers. The two most important ocean parameters that lend themselves to remote sensing are surface temperature and ocean color. Sea surface temperature has received much more attention from the remote sensing community, due to its importance in the energetics of meteorology, than has been given to the study of ocean color. It has only been within the last few years that the study of ocean color from high altitude aircraft has sufficiently demonstrated the potentialities of this parameter to lead to a spacecraft sensor. This sensor, the Costal Zone Color Scanner (CZCS) will be discussed later on.

The remote sensing of reflected solar and/or emitted thermal energy from the ocean has been used in a wide variety of studies with varying degrees of success. Topics that have been studied include:

1. Sea-surface temperature
2. Oceanic fronts
3. Currents
4. Costal upwellings
5. Pollutants including oil slicks, acid dumps, thermal effluents, and industrial discharge
6. Sediment transport
7. Aquatic vegetation mapping
8. Shallow-water bathymetry
9. Fish location
10. Sea-state via glitter pattern
11. Chlorophyll and yellow substance (or gelbstoife) concentration

Rather than becoming involved in a survey of the work done in each of these areas and the types of sensors used, the paper will first discuss the common elements of airborne and spaceborne systems, including the sensor, on-board data handling equipment, ground support systems, and ground data reduction. Secondly, equations for the design of visible and infrared imaging radiometers will be examined with emphasis on present practices and limitations. Then, two operational high-altitude airborne sensor systems and two spaceborne systems presently under development will be examined as examples of typical ocean surveillance designs. Finally, there will be a brief discussion of a few of the recent technological developments and their anticipated effect on the design and performance of visible and infrared radiometers through the mid-1980's.

Additional material on remote sensing of the ocean and the design and use of visible and thermal radiometers can be found in the literature and in several recently published books that survey the entire field of remote sensing. Outstanding among the latter is the Manual of Remote Sensing (1), a two volume 2100 page set of papers that address nearly every facet of remote sensing. The work was published in 1975 by the American Society of Photogrammetry and contains many references through 1973. Another excellent survey is the Remote

Sensing of the Environment (2) published in 1976 with over 1,000 references from the open literature, some as recent as 1975. Both the latter works and Remote Sensing of the Troposphere (3) published in 1972 contain excellent chapters on the remote sensing of the ocean that describe both recent research results and microwave, infrared, and visible sensors presently being used to conduct this research. Books specializing in infrared systems include Thermal Imaging Systems (4) by Lloyd and Infrared System Engineering (5) by Hudson. The former was published in 1975 and contains a very good discussion of all aspects of thermal imager design including detector arrays. The latter volume is more general in its approach and in addition, contains over 2100 references that are a comprehensive survey of the infrared literature prior to 1964. There are, of course, many additional books and articles concerned with remote sensors and their applications to oceanography, but these few references should provide sufficient background for someone new to the field to establish their bearings prior to moving on to the more specialized problem with which they may be concerned. Emphasis has been placed on publication dates in the above discussion due to the rapid pace with which the field is developing. In the short two-three years since some of these books were published, minor discrepancies have already appeared between discussed designs and current practices.

II. VISIBLE AND INFRARED IMAGING SYSTEMS

1. The Scanning Radiometer

The infrared scanning radiometer was developed principally because of the inability of film or image tubes to detect radiation of wavelengths greater than 0.7-0.8 micrometer and, as the need for visible and infrared radiometers arose, this type of sensor has been broadened to include visible channels thereby forming the class of multichannel visible and infrared scanning radiometers. Although these sensors ordinarily include both visible and infrared channels they may be designed to detect solely reflected solar or thermally emitted infrared energy, the most notable example of the former being the Multi-Spectral Scanner (MSS) of LANDSAT 1 and 2. This discussion will limit itself to those multichannel scanners in which the motion of the platform relative to the earth's surface provides one scan axis, thereby eliminating the two-axis scanners used with geostationary satellites.

Although, as a group, visible and infrared scanning radiometers consist of many varied designs, they, for the most part, do have certain common elements. Therefore it is possible to discuss in a general way the subsystems of a typical sensor. Such a collection of subsystems is shown in Figure 1. The following paragraphs are brief discussions of each of these subsystems.

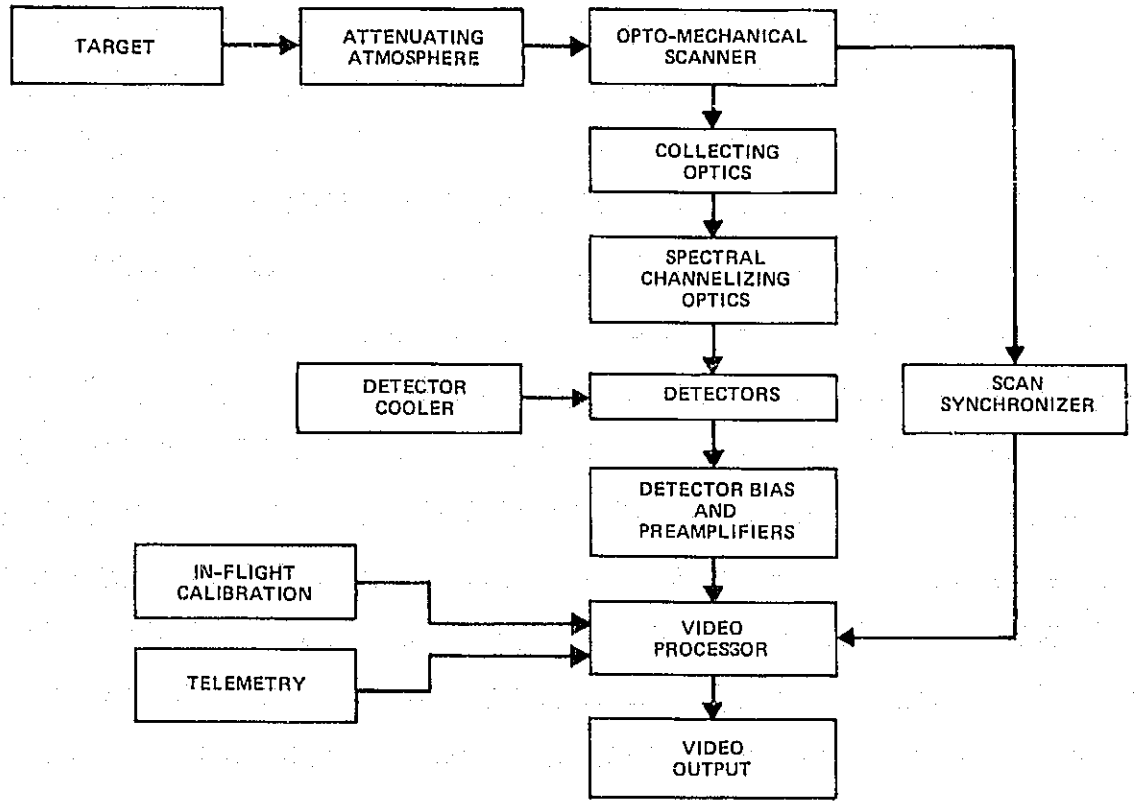

Figure 1. Scanning Radiometer Subsystems

The first two items shown, the target and attenuating atmosphere, are obviously external to the sensor. They are included because they are two of the dominant factors that govern the design of the radiometer. The target and the multichannel algorithm that will be used to separate out the parameters of interest in that target determine the required spectral position and width of the channels, the instantaneous-field-of-view (IFOV) and the required sensitivity of the sensor. However, the sensor design must also consider the contributions that the intervening atmosphere will have on the signal. In the thermal infrared portion of the spectrum the principal effect of the atmosphere on the upwelling radiation is molecular absorption. Therefore, in order to observe the surface, infrared channels are limited to "window" regions of the spectrum where there is very little water vapor (or trace constituent) absorption. The two major window regions are from 3.5–4.0 micrometers and 10.5–12.5 micrometers. For the visible portion of the spectrum, scattering of incident and reflected solar photons into the IFOV of the sensor by both aerosols and molecules is the

primary atmospheric effect. Therefore, when observing the color of the ocean as many as 98% of the photons reaching the sensor come from the atmosphere instead of the ocean. However, since this sky radiance is essentially constant for a given solar zenith and viewing angle, it can be subtracted from the sensor signal in order to expand the dynamic range of the desired ocean color signal.

Ordinarily the first element of the imager is the opto-mechanical scanner. This is typically an object plane scan mirror located in front of the collecting optics, there are image plane scanners that scan in the focal plane of the collecting optics, but all of the examples discussed later use object plane scanners. The optical element(s) of the scanner can be passive (flat mirrors) or active (lenses or curved mirrors). Most of today's scanners use flat mirrors the majority either inclined at 45° to the axis of rotation or in the form of a polygon perpendicular to the axis of rotation. Examples of both will be shown later. The major difference in these two systems is that with the inclined mirror system the projected image of the detector (or footprint) rotates as a function of twice the scan angle (measured from nadir). This is not very important unless the focal plane contains an array of detectors, then the relative orientation of their images on the surface will rotate with scan angle. Thus the footprint of a linear array with its long axis lying parallel to the direction of flight at nadir would be perpendicular to the flight direction at a scan angle of ±45°. This does not occur with the polygon scanner. It should, however, be recognized that both scan systems have geometrical distortions. Since the sensor is located at the center of a circle that is projected onto a flat or convex earth, the image will appear compressed near the edges. This effort can be compensated for by using a variable digital sampling rate, a variable speed scan mirror, or by correcting the data during processing on the ground. The latter is the usual solution. A second type of distortion is the increasing size of the footprint with scan angle. This is commonly referred to as the bowtie effect and can only be corrected by changing the IFOV with scan angle. This is not common but has been done. The scan mirror's speed of rotation is usually adjusted so that the along-track distance the surface nadir point moves is very nearly one IFOV per scan line period. Therefore, the lines are contiguous at nadir. However, due to the increasing size of the footprint with scan angle, the scan lines overlap at all other points.

The collecting optics generally consist of a reflecting cassegrain-type telescope, This serves as the entrance aperture to the sensor and, as shall be shown later, the area of the collecting optics plays a fundamental role in the sensitivity of the complete system.

There are two generally used methods to separate out that part of the spectrum desired for each channel; spectral reflectance or transmission filters and spatial dispersing elements such as prisms or interference gratings. Sensors having

several channels in both the visible and infrared portion of the spectrum may use a combination of both methods. The sensors described later use both techniques. In addition to these spectral elements, the channelizing optics include the transfer optics used to direct the photons from the focal plane of the collecting optics to the spectral separation elements, and the condensing optics that focus the spectrally delineated energy onto the detectors. The former, due to their broad spectral requirements are commonly all reflective elements, whereas the latter can be spectrally tailored transmissive optics.

The detectors for the type of sensor under consideration are point or discrete detectors as contrasted to imaging detectors such as the vidicon. The two most commonly used visible detectors (actually visible and near infrared) are the photomultiplier tube and the silicon photodiode. The latter with usable spectral response from 0.4 to 1.0 micrometers has gradually replaced the photomultiplier for most remote sensing applications. Infrared quantum detectors have been the subject of an intense research effort over the last 20 years which has resulted in a technology that is capable of producing very nearly background limited (blip) detectors over much of the infrared spectrum from 3-30 micrometers. As stated earlier, the growth of this technology is directly responsible for the rapid development of the scanning infrared radiometer.

Infrared detectors operating at wavelengths greater than 1.5 micrometer must be cryogenically cooled. Typical temperatures required for infrared detectors operating in the atmospheric windows at 3.5 and 11 micrometers are 77-110K. The three most commonly used methods for detector cooling are open cycle coolers in which the heat from the detector evaporates a liquid cryogen which is stored in a thermally insulated dewar, closed cycle refrigerators which typically use a two-stage compressor and an expansion valve near the detector, and radiative coolers which use the 3K space background as a heatsink. The first two of these are most often used with aircraft sensors where cryogen supplies or the power to drive a compressor are no problem. The radiative coolers have proven to be quite effective with spacecraft sensors. Other methods that have occasionally been used include solid cryogrens and thermoelectric coolers.

The detector preamplifiers are one of the most important elements in a visible and infrared radiometer. Their noise figure must be kept low enough for the limiting noise source of the system to be that of the detector, and this noise figure must be preserved through careful system design. Monolithic silicon detector arrays in which the preamplifier and the detector are part of the same silicon chip have very low noise figures. Similar infrared detector systems are under development.

The video processor amplifies the output from the detectors and preamplifiers, shapes the scan synchronizer pulse, blanks the signal from the preamplifiers during portions of the scan when it is not used, multiplexes the various ancillary signals onto the video, and outputs the analog video signal.

The scan synchronizer is a magnetic or optical encoder that is mechanically attached to the scan mirror shaft and serves as an indicator of the mirror's position. This is important both for internal timing in the video processor and for data reduction.

The radiometric accuracy of the imaging radiometer is limited by the accuracy of its calibration. It is especially important in the case of thermal channels that this calibration be updated periodically. This is accomplished by including the output of two or more blackbodies of known but different temperature in the video output. For an accurate calibration of the entire system these blackbodies should be viewed by the scan mirror and should fill the entrance aperture. Aircraft sensors ordinarily use two temperature controlled blackbodies that are viewed once each scan line. Spacecraft sensors typically use a single blackbody that is a portion of the base of the sensor and view space as a second calibration point. Since it is difficult to fabricate a uniformly diffuse visible source that will fill the entrance aperture of any sizable radiometer, the visible calibration is often performed by inserting the source at the focal plane of the collecting optics or by using laboratory calibration data.

Telemetry inserted into the video data stream is usually limited to that necessary for data reduction. Engineering telemetry is outputted via a separate data line. Typical video telemetry voltages include blackbody thermistor outputs, and staircase voltages to ascertain system linearity.

2. The Remote System

The scanning radiometer system, as mounted on the aircraft or spacecraft, includes important elements in addition to the sensor. These elements and their interrelation are shown in Figure 2. The multichannel scanning radiometer shown as the first element in this illustration includes the subsystems described in the previous section and diagramed in Figure 1. The following discussion will consider each of the subsystems of Figure 2.

The digitizer may be included as part of the radiometer or as a separate subsystem. There is usually a separate data line for each channel with all inputs to the digitizer being sampled simultaneously, at a predetermined rate converted by one or more A/D circuits, read into a buffer, and read out of the buffer serially, with a separate serial bit stream for each channel. The inputs to the buffers may be turned off during those portions of the scan in which there is no

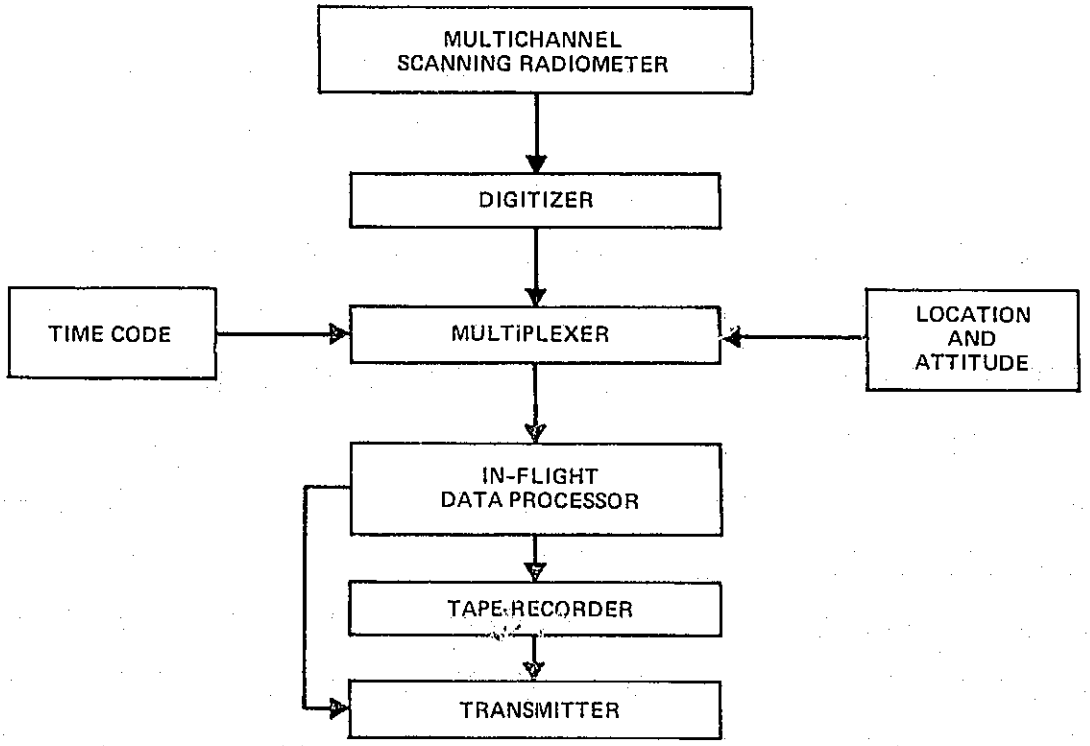

Figure 2. Scanning Radiometer Sensor System

useful video data, thereby reducing the system data rate considerably. The possible reduction in data rate will be dependent on the scan efficiency of the mechanism used and the field of view. Thus for a rotating inclined mirror system that scans ±45° about nadir, the data rate can conceivably be reduced to nearly one-fourth the rate resulting from digitizing at a constant rate during the complete revolution of the mirror.

The digitizer/buffer serial data streams enter the multiplexer where the data is interleaved and divided into convenient sized frames each of which has a header consisting of several data words reserved for identification, time code, platform location and attitude, and any other information that will aid in data reduction and analysis. The location and attitude data can be supplied by an inertial navigation system for airborne systems or calculated from ephemeris data for spacecraft systems.

The in-flight data processor can either be a microprocessor system designed to perform certain predetermined tasks such as ratioing or differencing of

channels or it may be a minicomputer that can be used to perform a wide variety of in-flight calibration and analysis tasks with the additional capability of being reprogrammed via ground commands.

The output from the processor can go either to a wideband tape recorder for storage or to a transmitter for relay to a ground station. Airborne data transmission can be used for real-time sensor performance checks and to aid in interaction with surface vessels.

3. Ground Equipment and Data Reduction

The typical scanning radiometer system described in the preceding two sections and diagrammed in Figures 1 and 2 requires a considerable amount of ground support equipment and a sophisticated data facility in order for the system to be maintained at the peak of its capability and to generate a useful end-product. The types of equipment required and the steps of a typical data calibration and analysis scheme are shown in Figure 3 and discussed in the following paragraphs.

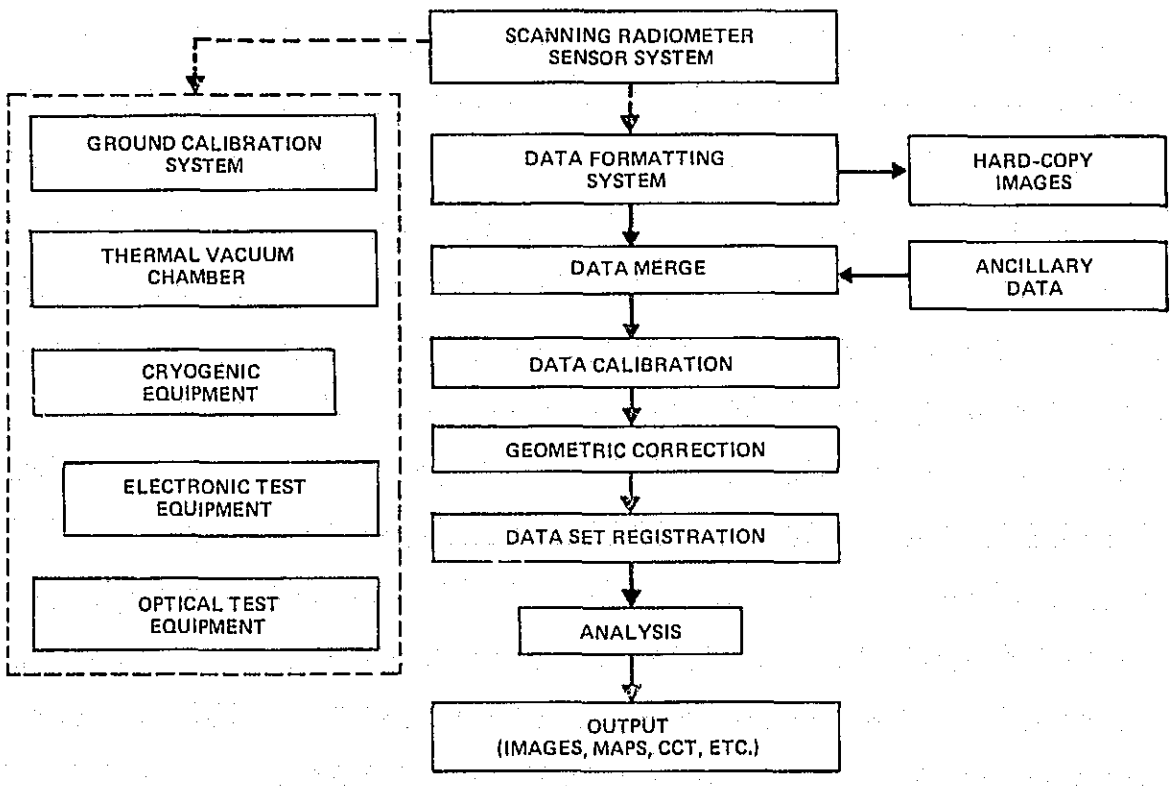

Figure 3. Scanning Radiometer Ground Equipment and Data Reduction Steps

The sensor calibration system includes secondary visible and infrared standard sources of a size to overfill the entrance aperture of the sensor. The most accurate visible source for this purpose is a large aperture integrating sphere suitably coated with a diffuse reflecting material and containing several quartz-iodide lamps that are shielded from a direct view of the sensor's entrance aperture (6). The spectral irradiance from the sphere is measured by comparison with a National Bureau of Standards calibrated quartz-iodide lamp using a spectrometer with a small integrating sphere and a thermopile detector. The infrared calibration source is a controlled, variable-temperature blackbody in a blackened cavity maintained at a temperature much less than the viewed surface. This source, which must also overfill the entrance aperture, is used to calibrate the in-flight blackbodies of the sensor which are, in turn, used to calibrate the data. Great care must be taken to make the surface a near-perfect emitter, to maintain a uniform temperature across the surface, and to measure the surface temperature with the required accuracy.

The thermal vacuum chamber serves to simulate the environment that the sensor will be subjected to including atmospheric pressure, temperature, and, in some cases, radiant sources. The chamber must be capable of holding both visible and infrared sources in order to ascertain the effects of environmental extremes on the sensor's performance. This is especially true for infrared sensors since a change in instrument temperature will result in a change in the radiant energy emitted to and reflected by the in-flight blackbodies, thereby changing their calibration.

Cryogenic equipment that may be required includes liquid cryogen storage and transfer gear for sensors with dewars and for cooling of vacuum walls, closed-cycle liquid helium refrigerators with blackbody panels to simulate space for bringing radiative coolers to their operating point during vacuum chamber testing and to give a simulated space view which is used as one of the in-flight infrared calibration points, dewars to align and check infrared optics and detectors prior to mounting in the sensor, and clamp-on bench coolers for operating radiative coolers outside the vacuum chamber.

In addition to the normal electronic test equipment contained in any well-equipped laboratory, a remote sensing laboratory should also include a detector test console, digital test gear, time code generator/translator, and computer-controlled test console for use during sensor testing and calibration.

The major piece of optical test equipment needed is an all-reflective optical collimator with an entrance aperture wide enough to fill all anticipated radiometers and a set of visible and infrared focal plane targets for measuring the modulation transfer function (MTF) of the sensor. A spectrally scanning source

of nearly monochromatic radiation is also required in order to measure the spectral response of each channel. In most cases a grating spectrometer is adequate.

The first step in reducing the scanning radiometer data to a useful product is to reformat the multiplexed serial data into computer compatible tapes (CCT's). In the case of some aircraft sensors this step is performed by the in-flight data processor. The CCT's can be used to generate an image tape which in conjunction with an electronic image processor can be used to generate images on a television screen, film, or photosensitive paper, in order to check the quality of the data.

Since the data rate of this type of sensor is often quite high, the data may have been recorded on several serial tracks of an in-flight or ground tape recorder. It is, therefore, necessary that these data sets be merged to form a single time-series of CCT's. This can be done as an integral part of the reformatting process or as a separate step. Also, at this point, other data sets such as surface-truth, calibration data, orbit information, and data from other sensors can be merged into the data set.

Data calibration consists of using the calibration information obtained during preflight calibration, from inflight calibration, and, in the case of airborne sensors, post-flight values to convert the digital counts to values of radiant intensity.

Geometric corrections are used to remove the distortions of the image caused by the inherent performance of the scan mechanism. As stated previously, these distortions can be eliminated by various modifications of the basic sensor design. However, these modifications complicate the sensor design to such an extent as to imperil reliability and are therefore not justified in most cases. Corrections performed by the ground data system can range from simple pixel averaging schemes to multi-dimensional interpolation.

The major reason for geometric fidelity is to allow the sensor data to be registered with other data sets such as that from other imagers, surface sensor data, and various parameter and feature maps. This process typically involves matching the sensor data to a digital base map.

Multichannel analysis is essentially converting a series of radiances measured at the sensor to a smaller set of surface parameters. This analysis is performed by algorithms developed via modeling and laboratory and field experiments. Several current schemes will be mentioned in the discussions of specific scanning radiometers.

After the data analysis has converted the sensor output to the required surface parameters, they, in turn, must be put into the form most convenient for the ultimate user. Types of output include visual displays, radiance images, thematic images, maps, computer compatible tapes, and catalogs.

III. SCANNING RADIOMETER DESIGN

The application of remote sensing to the detection of oceanographic parameters that are of interest to the scientific, commercial, and/or military communities consists of four major phases; (1) problem delineation, (2) multichannel algorithm development, (3) sensor design and construction, and (4) data collection and reduction. This section, concerned with the first part of (3), assumes that (1) and (2) have taken place and have resulted in a set of spectral channel positions and half-widths, desired footprint and swath width, required sensitivity, and probable platform. This information, as shall be shown, is sufficient to enable the development of a preliminary system design. The following paragraphs will develop the sensitivity equation for both visible and infrared channels and thereby demonstrate which elements of the scanning radiometer govern its design and what tradeoffs can be made.

A commonly used performance criteria is the peak-signal to rms-noise ratio (SNR) which can be defined by

$$\frac{S}{N} \equiv \int_{\lambda_1}^{\lambda_2} \frac{P_\lambda d_\lambda}{(NEP)_\lambda} \tag{1}$$

where λ_1 and λ_2 are the wavelength limits of the particular channel under consideration, P_λ is the spectral irradiant power received by the detector, and $(NEP)_\lambda$ is the spectral noise equivalent power. P_λ is given by

$$P_\lambda = aA\Omega\tau(\lambda)N_\lambda \tag{2}$$

where a is the albedo for reflected solar channels and the emissivity for thermal channels. The emissivity is assumed to be unity for thermal channels viewing water surfaces. A is the area of the entrance aperture of the sensor including losses due to obscuration of the primary mirror by the secondary. Ω is the

solid angle subtended by the instantaneous field of view (IFOV). τ (λ) is the wavelength dependent transmission of both the atmosphere and the sensor optics, and N_λ is the spectral radiance from the IFOV.

If the spectral bandwidth of the channel does not include strong atmospheric absorption lines and the spectral response of the sensor is constant over the bandwidth, a valid assumption is that:

$$\tau(\lambda) = \tau_0 \text{ for } \lambda_1 \leqslant \lambda \leqslant \lambda_2$$

and

$$\tau(\lambda) = 0 \text{ for } \lambda_1 > \lambda > \lambda_2$$

Thus,

$$\frac{S}{N} = a A \Omega \tau_0 \int_{\lambda_1}^{\lambda_2} \frac{N_\lambda}{(NEP)_\lambda} \, d\lambda \tag{3}$$

Equation (3) is true for both reflected solar and thermal channels. It is only when calculations are made for the noise equivalent power for channels in the different wavelength regions, which consequently necessitates different types of detectors, that the sensitivity equations begin to deviate from one another.

A sensitivity criteria used primarily with infrared detectors, the specific detectivity or D* is defined as

$$D^*(\lambda) \equiv \frac{(A_d \Delta f)^{1/2}}{(NEP)_\lambda} \tag{4}$$

Where A_d is the area of the detector and Δf, the output bandwidth, is given by

$$\Delta f = \frac{1}{2t_d} \tag{5}$$

where t_d is the IFOV dwell time which, for scan lines contiguous at nadir, is given by

$$t_d = \frac{h\Omega}{2\pi v} \tag{6}$$

where h is the altitude of the sensor platform, Ω is the solid angle subtended by the IFOV, and v is the surface speed of the sensor platform.

Equations (3) and (4) can be combined to give

$$\frac{S}{N} = \frac{A\Omega\tau_0}{(A_d \Delta f)^{1/2}} \int_{\lambda_1}^{\lambda_2} D^*(\lambda) N_\lambda \, d\lambda \tag{7}$$

where the emissivity, a, is assumed as unity.

For the thermal infrared channels, the most commonly used sensitivity criteria, instead of the signal to noise, is the noise equivalent temperature difference (NETD). This quantity is usually difined as being that small change in temperature of a blackbody target which will result in a peak-signal to rms noise ratio of unity as measured at the output of the sensor. Since a small change in temperature is equivalent to a small change in radiance, N_λ of equation (7) becomes dN_λ and

$$dN_\lambda = dT \frac{dN_\lambda(T)}{dT} \approx \Delta T \frac{dN_\lambda(T)}{df}. \tag{8}$$

Combining equations (7) and (8) and the definition of NETD results in

$$\text{NETD} = \frac{(A_d \Delta f)^{1/2}}{A \Omega \tau_0} \left[\int_{\lambda_1}^{\lambda_2} D^*(\lambda) \frac{dN_\lambda(T)}{dT} d\lambda \right]^{-1} \tag{9}$$

For $\lambda T < 4000$ $\mu m\,^\circ K$, Planck's law may be approximated by Wien's radiation law and

$$\frac{dN_\lambda(T)}{dT} = \frac{c_1 N_\lambda(T)}{\lambda T^2} \tag{10}$$

where

$$c_1 = 1.4388 \times 10^4 \ \mu m\,^\circ K$$

Therefore

$$\text{NETD} = \frac{(A_d \Delta f)^{1/2} T^2}{A \Omega \tau_0 c_1} \left[\int_{\lambda_1}^{\lambda_2} N_\lambda(T) D^*(\lambda) \frac{d\lambda}{\lambda} \right]^{-1} \tag{11}$$

For the case of photodetectors having theoretical performance such that

$$D^*(\lambda) = \frac{\lambda}{\lambda_p} D^*(\lambda_p) \quad \text{for } \lambda \leq \lambda_p$$

and

$$D^*(\lambda) = 0 \qquad \text{for } \lambda > \lambda_p$$

equation (11) can be simplified to

$$NETD = \frac{(A_d \Delta f)^{1/2} T^2 \lambda_p}{A \Omega \tau_0 c_1 D^*(\lambda_p)} \left[\int_{\lambda_1}^{\lambda_2} N_\lambda(T) d\lambda \right]^{-1} \tag{12}$$

This form of the NETD equation is quite convenient. The integral is evaluated numerically. It should be kept in mind that the NETD is a function of T and that any specification of the NETD of a sensor without quoting the target temperature at which it was calculated or measured is meaningless. Typically the NETD is given for a 300K scene.

In the case of visible or near-infrared channels using silicon photodiodes, the noise-equivalent-power can be expressed as

$$NEP = \frac{1}{S} (i_s^2 + i_d^2 + i_r^2)^{1/2} \tag{13}$$

where

S = diode responsivity in ampere/watt

i_s = shot noise current due to signal flux on the detector

i_d = photodiode leakage current noise when not illuminated

i_r = load resistor Johnson noise current.

The noise currents are given by:

$$\begin{aligned} i_s^2 &= 2eI_s\Delta f \\ i_d^2 &= 2eI_d\Delta f \\ i_r^2 &= 4KT\Delta f/R \end{aligned} \tag{14}$$

where

I_s = signal current

I_d = dark current

R = load resistor

Δf = output bandwidth (see equations (5) and (6)).

Since in Equation (14) only the signal current is a function of wavelength and it is calculated using the minimum detector illumination, equations (3) and (13) give

$$\frac{S}{N} = \frac{a A \Omega \tau_0 S}{(i_s^2 + i_d^2 + i_r^2)^{1/2}} \int_{\lambda_1}^{\lambda_2} N_\lambda \, d\lambda \tag{15}$$

where N_λ is now the solar spectral radiance and the integral can be extracted from various solar constant tables such as Thekaekara (6), Johnson (7) or Labs and Neckel (8). Strictly speaking, a and S are also functions of λ, but an average value can be readily determined for a given spectral bandwidth with no appreciable loss in accuracy.

Equations (12) and (15) can be used to calculate the performance of the various channels of a visible and infrared scanning radiometer design and to adjust the

parameters of that design if it fails to meet the sensitivity required for the desired sensor application. These equations however, assume certain ideal conditions that are modified by reality and neglect certain effects that tend to degrade the performance of the sensor. These effects can be put in the form of a degradation factor, a, which, when multiplied with the NEP, results in a decrease in the sensor sensitivity. Goldberg (7) has identified six multiplicative factors which may contribute to a. These include:

a_1 - detector operating conditions other than those under which D* (or S) was measured.

a_2 - effective noise bandwidth including $\frac{1}{f}$ noise

a_3 - radiation or electronic chopping

a_4 - electronic filter response

a_5 - system noise (primarily amplifier noise)

a_6 - diffraction effects.

Obviously, some of these factors are not applicable to the type of sensor being considered. For instance, the Advanced Very High Resolution Radiometer (AVHRR) design (8), which will be examined in a later section, found that only a_2 and a_5 were significant and that these resulted in $a = 1.6$. Goldberg (7) has demonstrated that in some cases, a may be as large as 13.9. For the type of sensor under discussion the value of a for the AVHRR is more typical.

Thus, equations (12) and (15) when modified by a should give a reasonably accurate estimate of sensitivity that can be expected for a particular sensor design. The sensor itself as was discussed in the preceding section, is only a portion of the complete sensor system and, therefore, the sensor design must be compatible with the total system. With the advent of multichannel scanning radiometers having more channels, smaller IFOV's and wider scan swaths, the factor that impacts system design the most is data output. In fact, in most cases the ability to store, transmit to the ground, and analyze the data from the sensor determines the system design limits rather than the design being governed by state-of-the-art sensor technology.

The data rate, d, from a scanning radiometer is given in bits/second by

$$d = \frac{ncb}{t_d} \tag{16}$$

where n is the number of channels, c is the number of samples/IFOV, b is the number of binary bits used to represent each analog sample, and t_d is the dwell time per IFOV.

Combining equations (6) and (16) gives

$$d = \frac{2\pi ncbv}{\Omega h} \tag{17}$$

Since the Nyquist criteria calls for a minimum of 2.5 samples/cycle and since at least two IFOV are required for a complete cycle (black to white or hot to cold), a commonly used value for c is 1.4. The value of b is determined by the sensitivity and range of the sensor and is typically 8 or 10.

An example of the data rates resulting from today's scanners can be had by examining the Coastal Zone Color Scanner (9) slated for a 1978 launch aboard Nimbus-G. The parameters used with equation (17) are

$n = 6$

$c = 1.4$

$b = 8$

$v = 6.45$ km/sec.

$\Omega = 7.48 \times 10^{-7}$ st.

$h = 925$ km

which results in

$d = 3.94 \times 10^6$ bits/second

or 2.4×10^{10} bits/orbit which is an order of magnitude larger than available space-qualified tape recorders. Thus, the data must be reduced by onboard processing or the on-time of the sensor limited to those periods that the spacecraft is in contact with a ground station.

IV. OCEAN TEMPERATURE SCANNER

The Ocean Temperature Scanner (OTS) is a 5-channel scanning radiometer designed for use aboard medium and high altitude aircraft. The sensor was designed, fabricated, and tested by personnel of the National Aeronautics and Space Administration's Goddard Space Flight Center (10) and has been flown aboard a CV-990 and a U-2 aircraft at altitudes of 11 km and 19.8 km, respectively. This sensor is, in many aspects, a simulator of the Advanced Very High Resolution Radiometer Mod 2 (AVHRR/2) that will be discussed later and is presented here both because it is typical of airborne sensors used to develop spacecraft systems and because of several unique design characteristics.

Table 1 lists some of the design parameters of the OTS. The 3.5 or 7.0 milliradian field of view is determined by the appropriate transfer optics between the focal plane of the 12.5 cm diameter Dall-Kirkham telescope and the detector chips which serve as the limiting aperture for both the infrared and visible channels. Two IFOV's are used in order to achieve approximately the same 70-meter footprint from both medium and high altitude. The difference in scan speed and mirror speed in Table 1 is due to the use of the double-sided scan mirror shown in Figure 4. The scan mirror has its axis of rotation parallel to the direction of flight. As seen in Figure 4, the optical path is from the scan mirror, off a large folding mirror, into the telescope, through the transfer optics, and into the LN_2 dewar where the 4 infrared detector chips are located, each with a bandpass filter immediately in front of it. A two-dimensional view of the optics is shown in Figure 5, which also illustrates the location of the visible detector and its bandpass filter. The visible light is focused on the detector by using the first uncoated germanium relay lens as a concave mirror. The array of infrared detectors is arranged such that its long axis is along the scan line. Thus, the IFOV of the first detector is viewed by the following detectors a few milliseconds later.

Table 2 lists the spectral channels of the OTS and their function. Of principal interest are Channels 3 and 4, the two atmospheric windows in the thermal infrared. Although both of these channels are relatively free of water vapor absorption, the small amounts remaining are sufficient to cause errors in the range of 2-8 K in determining the sea surface temperature. Prabhakara et al. (11) have shown that the difference in absorption in Channels 3 and 4 can be used to linearly extrapolate the temperatures measured by these channels to zero

Table 1

OTS Design Parameters

Number of Channels	-- 5 (4 IR, 1 Vis)
Instantaneous Field of View (IFOV)	-- 7.07 or 3.53 mr.
Field of View	-- ±30°
Scan Speed	-- 3.12 Lines/sec
Mirror Speed	-- 1.56 Hz
Range (adjustable)	-- 230 - 330°K (IR)
	-- 0-20% Albedo (Vis)
Sensitivity	-- NETD (7 mr) = 0.2K @ 300K NETD (3.5 mr) = 0.4K @ 300K (Channel - 4 measured)
In-Flight Calibration (IR)	-- (a) 35°C Regulated blackbody (Clamp)
	-- (b) Unregulated blackbody (variable temperature)
In-Flight Calibration (Vis)	-- Zero-level clamp on blackbody

Table 2

OTS Channels

Channel	Detector Material	Temperature Range	NETD (°K) (Calculated)		Purpose
1 3.6 – 4.1 μm	HgCdTe	280 – 330	0.33	0.72	atmospheric window
2 6.5 – 7.0 μm	HgCdTe	280 – 330	0.09	0.20	H_2O vapor detection
3 10.2 – 11.2 μm	HgCdTe	280 – 330	0.05	0.11	atmospheric window
4 11.9 – 12.9 μm	HgCdTe	280 – 330	0.07	0.15	atmospheric window
5 0.5 – 0.9 μm	Silicon	S/N ≈ 1000	7 mr optics	3.5 mr optics	discern cloud contaminated data

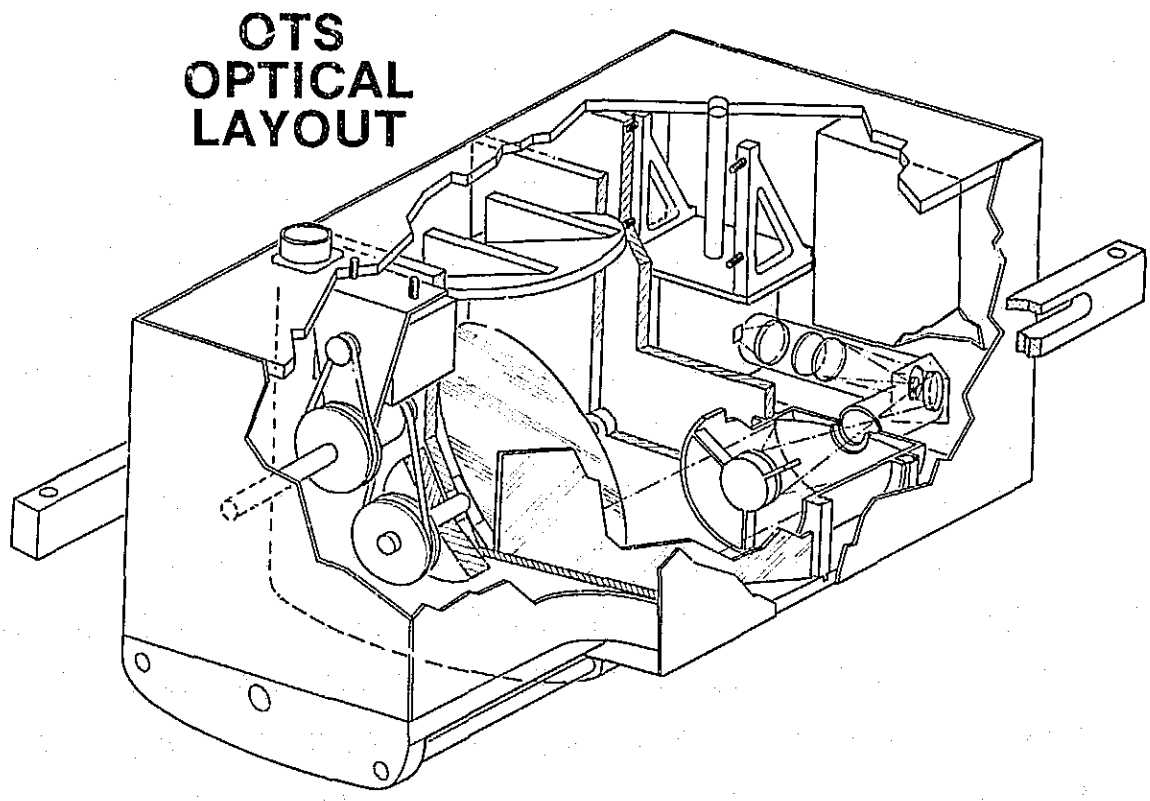

Figure 4. OTS Optical System Schematic

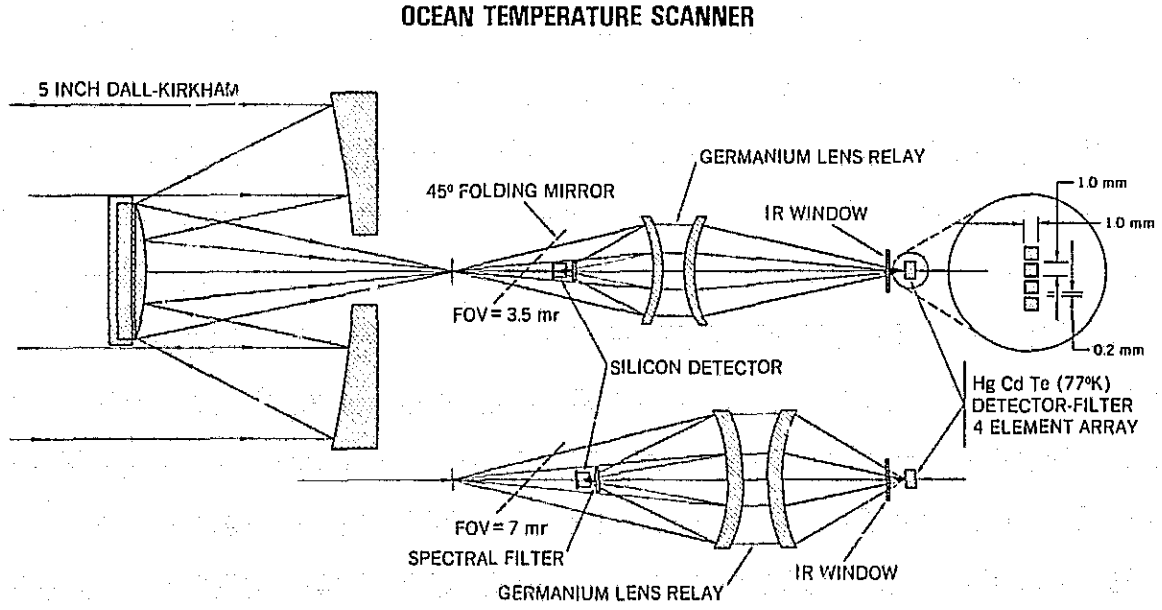

Figure 5. 3.5- and 7-Milliradian Transfer Optics

absorption which is equivalent to the true surface temperature. Thus, these channels are included in the OTS in an effort to ascertain the accuracy of this correction and to support the AVHRR/2, which includes these same channels. It may well be that Channel 1 (3.5-4.0 micrometers), which is an atmospheric window with even less water vapor absorption than Channels 3 or 4, can serve as a third point for this extrapolation. Unfortunately, there is enough reflected solar energy in Channel 1 that it would probably be limited to nighttime use.

V. OCEAN COLOR SCANNER

The Ocean Color Scanner (OCS) (12) is a 10-channel airborne scanning radiometer designed to image reflected solar energy in the range 0.4-1.0 μm. As was the case with the OTS, this sensor was designed, fabricated, and tested by personnel of NASA's Goddard Space Flight Center. Three duplicate models of the OCS have been assembled to date; they have flown on an F-106, Lear jet, U-2, and Mystere-20 Falcon. The latter aircraft was used to support ocean color experiments by the Joint Research Center, European Communities, off the coast of Holland in the Summer of 1977. Problems that have been studied using data from the OCS include bioproductivity, acid waste dumps, sediment transport, oil spills, and red tide blooms. The sensor's major function is to support algorithm development for the Coastal Zone Color Scanner (CZCS) (9) slated for launch aboard Nimbus-G in 1978.

Tables 3 and 4 list some of the OCS design and performance parameters. The aircraft parameters are from the U-2, this being the platform used for the majority of the flights due to its ability to fly above most of the atmosphere and the synoptic coverage from these attitudes. Figure 6 is a schematic of the OCS optics. The 45° inclined scan mirror is not shown. From the focal plane of the 12.5 cm diameter Dall-Kirkham telescope, the light enters a grating spectrometer which has 24 bundles of glass fibers in its focal plane. Ten of these bundles, positioned so as to cover the spectral intervals shown in Table 4, go to order-isolating filters, optical relays, and silicon photodiodes. The 14 remaining spectral channels can be interchanged with any of the ten output channels as needed.

A photograph of the OCS is shown in Figure 7, with the various components labeled. Nadir is towards the top of the photograph. During flight operations, the scanner is enclosed in a semi-cylindrical cover approximately 75 cm long and 25 cm diameter. The scanner mass is approximately 34 kg.

Table 3

Radiometer Data

Aircraft Speed	201 meter/sec (390 knots/hour nominal)
Aircraft Altitude	19.8 kilometers (nominal)
Angular Resolution (IFOV)	3.5 mr
Footprint	70 m × 70 m
FOV	±45°, from nadir
Scan Rate (mirror speed)	2.727 revolutions/sec.
Swath Width	39.6 kilometers
Output Voltage	0 volts to +5 volts
Scanner Information Output	0 volts to +4 volts
Output Bandwidth	0 to 2500 Hertz
Output RMS Noise Level	10 millivolts

Table 4

Optical Parameters of the Ocean Color Scanner Channels

Channel	Center Wavelength (nm)	Full Width at Half-Height Bandwidth (nm)	Radiance (Gain × 1) $mw/cm^2\ \mu$
1	431	22.5	80.25
2	472	21.5	65.80
3	506	27.5	42.37
4	548	24.5	26.00
5	586	25.8	19.90
6	625	26.0	15.73
7	667	25.8	12.20
8	707	23.2	9.95
9	738	22.5	126.7
10	778	23.0	6.74

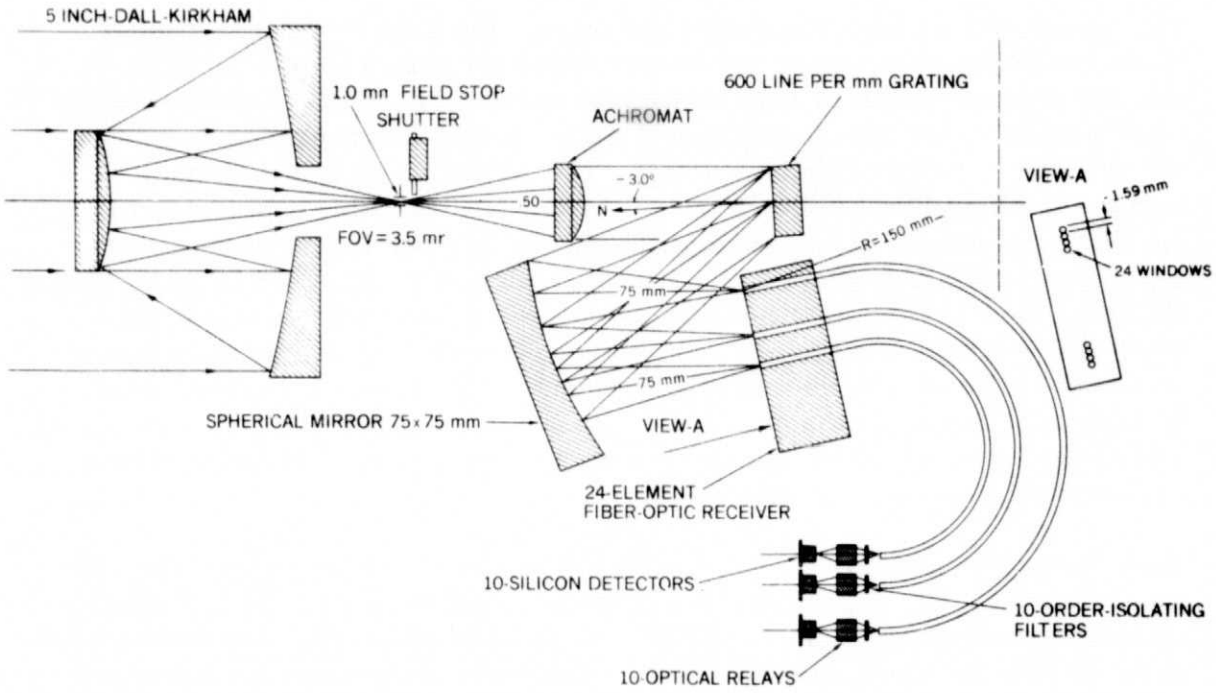

Figure 6. Ocean Color Scanner Optics

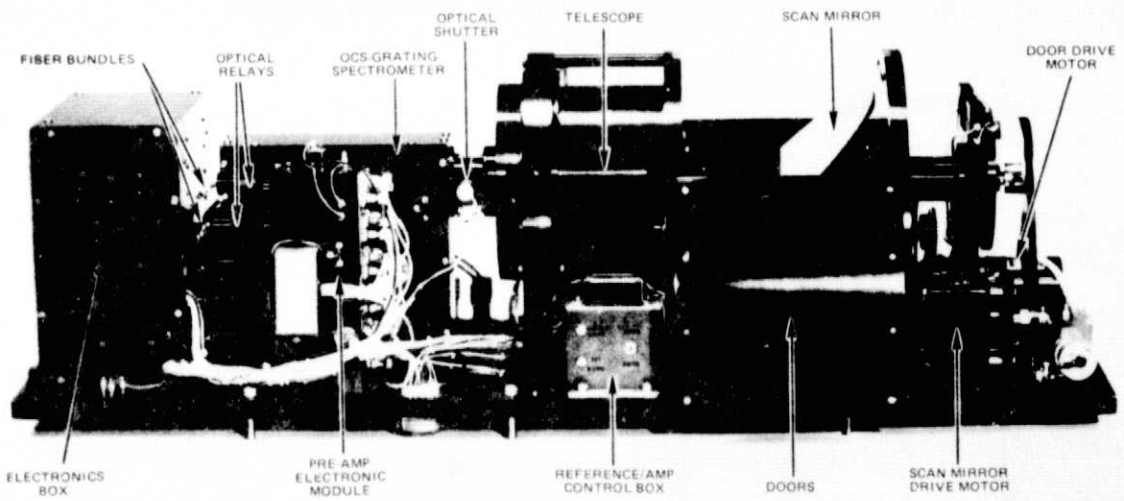

Figure 7. Airborne Ocean Color Scanner

VI. ADVANCED VERY HIGH RESOLUTION RADIOMETER — MOD 2

The Advanced Very High Resolution Radiometer (AVHRR) (13) is a 4-channel visible and infrared scanning radiometer slated for launch aboard the first of the TIROS-N spacecraft in 1978 (which shall be designated NOAA-A when turned over to the National Oceanographic and Atmospheric Administration as part of the operational meteorological system). The AVHRR/2 (8) is a 5-channel version of the AVHRR that will be aboard NOAA-C in 1979 and is expected to be the NOAA operational polar-orbiting visible and infrared imager through the mid-1980's. The AVHRR or AVHRR/2 will replace the VHRR and SR of the present NOAA series. The AVHRR/2 and the Coastal Zone Color Scanner (CZCS) (9), which will be discussed next, are state-of-the-art designs for spaceborne visible and infrared scanning radiometers and are presented here as solutions to specific problems and as examples of present technology. Different objectives may require radically different designs from these, but the discussion of Sections II and III will apply in most instances.

All of the pertinent details of the AVHRR/2 are given in Table 5 (14). The 450 nm orbit and 1.3 mr IFOV result in a 1 km footprint with, as noted in Table 5, all channels co-registered to within 0.1 mr in each axis. The first flight model of the AVHRR has completed all testing and has met the requirements (where applicable) listed in Table 5; it is not expected that the AVHRR/2 will have any

Table 5

Summary
Advanced Very High Resolution Radiometer—Mod 2
AVHRR/2

MISSION PARAMETERS

- ORBIT ALTITUDE — 450 N.M.
- ORBIT INCL — 98.8°
- ORBIT PERIOD — 102 MIN.
- ASCEND. NODE — 3:30 PM
- EARTH ORIENTED — ±1 DEG
- GROUND SPEED — 3.5 NM PER SEC
- FIRST LAUNCH — NOAA-C 1979
- SUN ANGLE — 0°-68° FROM PITCH AXIS

AVHRR/2 SYSTEM CHARACTERISTICS

GENERAL

- 5 CHANNEL SCANNING RADIOMETER, 8" OPTICAL SYSTEM, VIS AND IR CAPABILITY

- PHYSICAL: 30.75 X 14.5 X 11.5 INCHES, 65 POUNDS PER INSTRUMENT
- ELECTRICAL: 28.5 WATTS @ 28 VDC, + 10 VDC + 5 VDC (SCAN MOTOR IN HIGH POWER MODE)
- DATA OUTPUT: 10 BIT DIGITAL: S – BAND: 600 kbps DAY, 300 kbps NITE, REAL TIME AND STORED
  VHF: APT TRANSMISSION
- THERMAL OPERATING RANGE: 10°-30°C; LOUVER CONTROLLED AT +15°C
- STATUS: FLYABLE PROTOFLIGHT AVAILABLE 2nd QCY 1978 MANUFACTURER–ITT A/OD FT. WAYNE, IND.

SCANNER

- 360 RPM, 80 POLE HYSTERESIS SYNCHRONOUS, ≤17 μsec JITTER (~½ IFOV)
- ELLIPTICAL BERYLLIUM SCAN MIRROR

ELECTRICAL

- 10 BIT A/D CONVERTER, SIMULTANEOUS SAMPLE AND HOLD, SEQUENTIAL CONVERSION AND READOUT
- 28 COMMANDS
- 22 ANALOG HOUSEKEEPING PARAMETERS
- 14 DIGITAL TELEMETRY

COOLER

- 2 STAGE PASSIVE RADIANT COOLER FOR 3 IR DETECTORS
- DESIGN TEMP. 98°K; OPERATING TEMP. 105°K/108°K SELECTABLE
- DEPLOYABLE COVER/EARTH SHIELD–SINGLE ACTION
- BENCH CHECK CAPABILITY @ 108°K

OPTICS

- 6 INCH AFOCAL, ALL REFLECTIVE, CASSEGRAINIAN TELESCOPE
- PRIMARY: PARABOLOID, 8 IN APERTURE, CERVIT, F_L = 10 INCHES
- SECONDARY: PARABOLOID, 1 IN APERATURE, CERVIT, 8 X MAG. OBSC. 6%
- INTERVERTEX DISTANCE 8.75 IN.
- POLARIZATION < 7%

PERFORMANCE	CH 1	CH 2	CH 3	CH 4	CH 5
SPECTRAL RANGE	0.58-0.68μ	0.725-1.0μ	10.3-11.3μ	3.55-3.93μ	11.5-12.5μ
DETECTOR TYPE	SILICON	SILICON	HgCdTe	InSb	HgCdTe
RESOLUTION	← 0.59 NM →				
IFOV	← 1.3 MA X 1.3 MR →				
REGISTRATION	← WITHIN 0.1 MR IN EACH AXIS →				
S/N	3:1	3:1	(@ ρ = 0.5%)		

Table 5 (Cont'd)

NETD	N/A	N/A	≤0.12°K @ 300°K
MTF (@ 1 IFOV)	0.30		
DYNAMIC RANGE	0.5% to 100% ALBEDO		4°K to 320°K

difficulty in performing to these same specifications. A photograph of the AVHRR is shown in Figure 8 with nadir towards the top of the figure. Since AVHRR and AVHRR/2 are externally indistinguishable, this figure can serve for either. Figure 9 is an exploded view of the sensor broken down into its five basic modules. The black area on the baseplate serves as the in-flight calibration blackbody. The deep notch on the cooler side of the scan cavity allows the sensor to view deep space which serves as a second calibration point for the infrared channels and as a zero-clamp for both visible and infrared channels. The door on the passive cooler remains closed until 1-2 weeks after launch to prevent contamination of its heat-emitting surfaces by volatiles outgassed by the spacecraft and its sensors and then serves as a shield to prevent cooler from viewing the earth or its atmosphere.

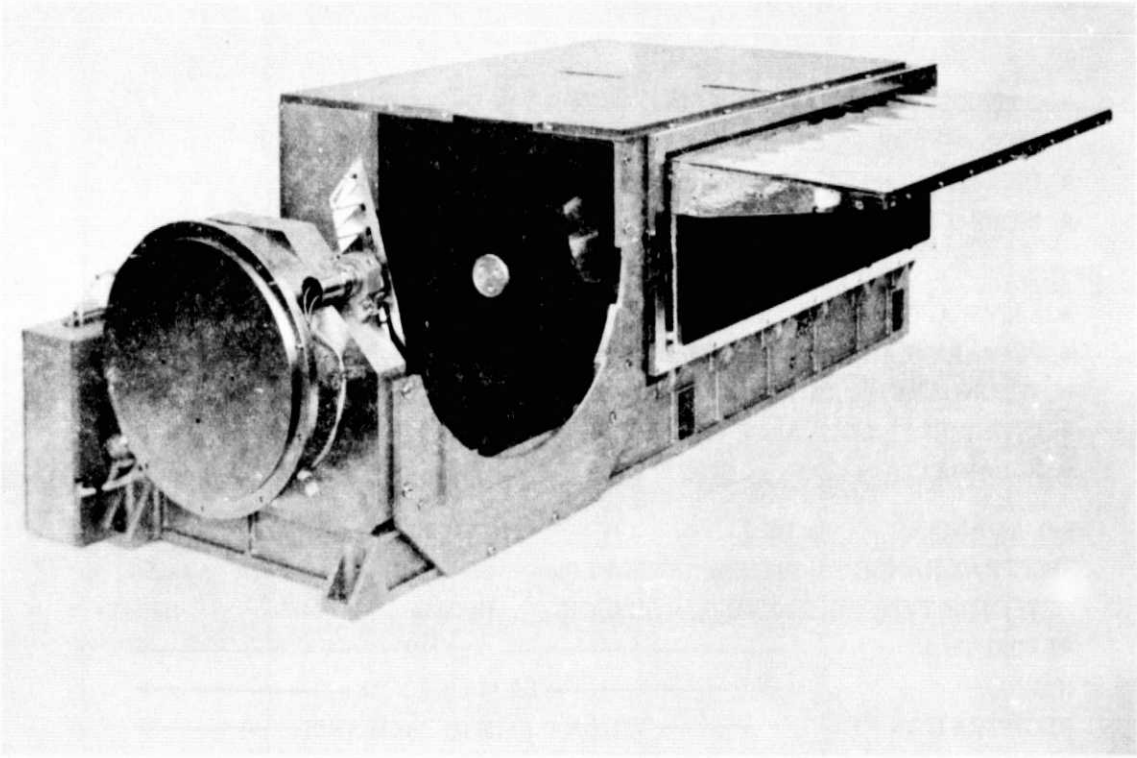

Figure 8. AVHRR

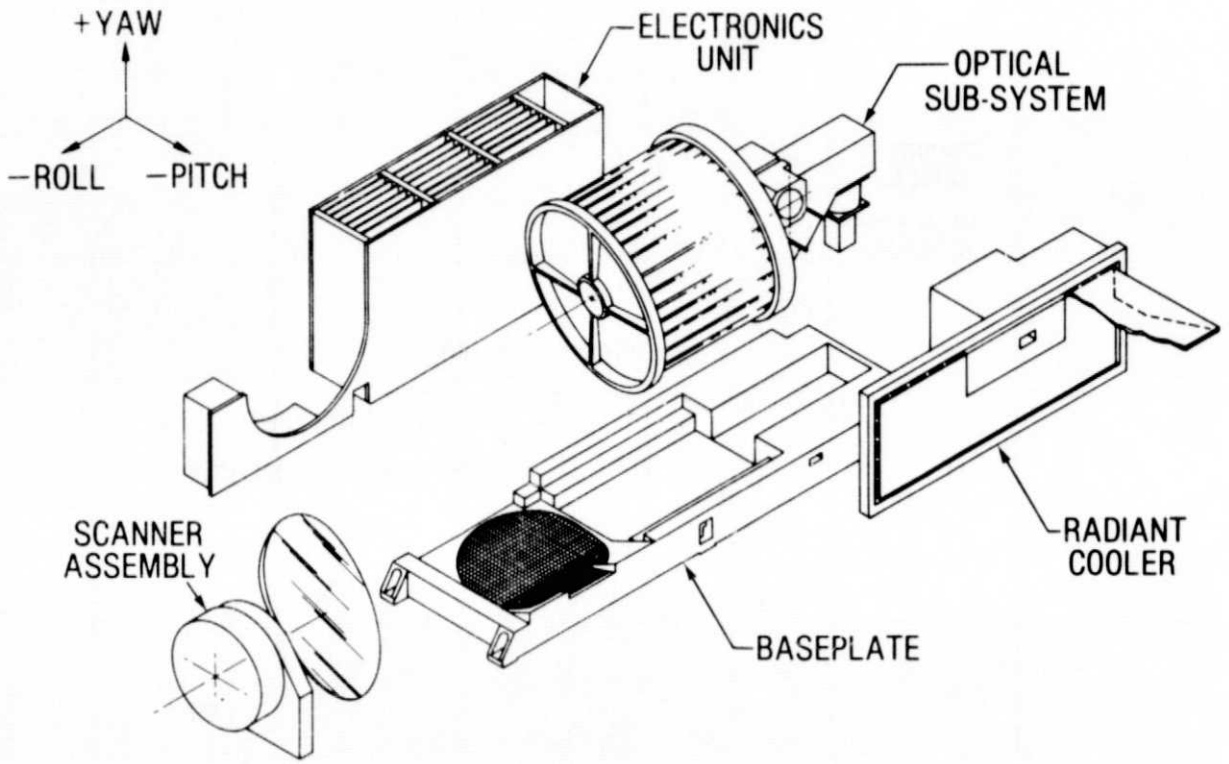

Figure 9. AVHRR/2 Basic Modules

Figure 10 shows all of the optical elements of the AVHRR/2 except the scan mirror. Elements labeled M are mirrors, F are filters, W are windows, L are lenses, and D are dichroic filters. The box labeled "vacuum" is the back of the passive cooler which is operable in the laboratory by placing an evacuable LN_2 cooler over its front surface.

The AVHRR/2 is destined to supply data for a wide variety of meteorological, hydrological, and oceanographic parameters, but the major reason for adding the fifth channel was to insure the AVHRR's capability of measuring global sea surface temperature to an absolute accuracy of less than 1.0 K using the technique discussed in Section IV.

VII. COASTAL ZONE COLOR SCANNER

The Coastal Zone Color Scanner (CZCS) (9) is a six channel scanning radiometer slated for launch aboard Nimbus-G in October, 1978 and is expected to make measurements in both coastal and open ocean for the purpose of observing chlorophyll concentrations, yellow stuff, surface vegetation, and surface temperature. The CZCS is the first spacecraft sensor dedicated to the study

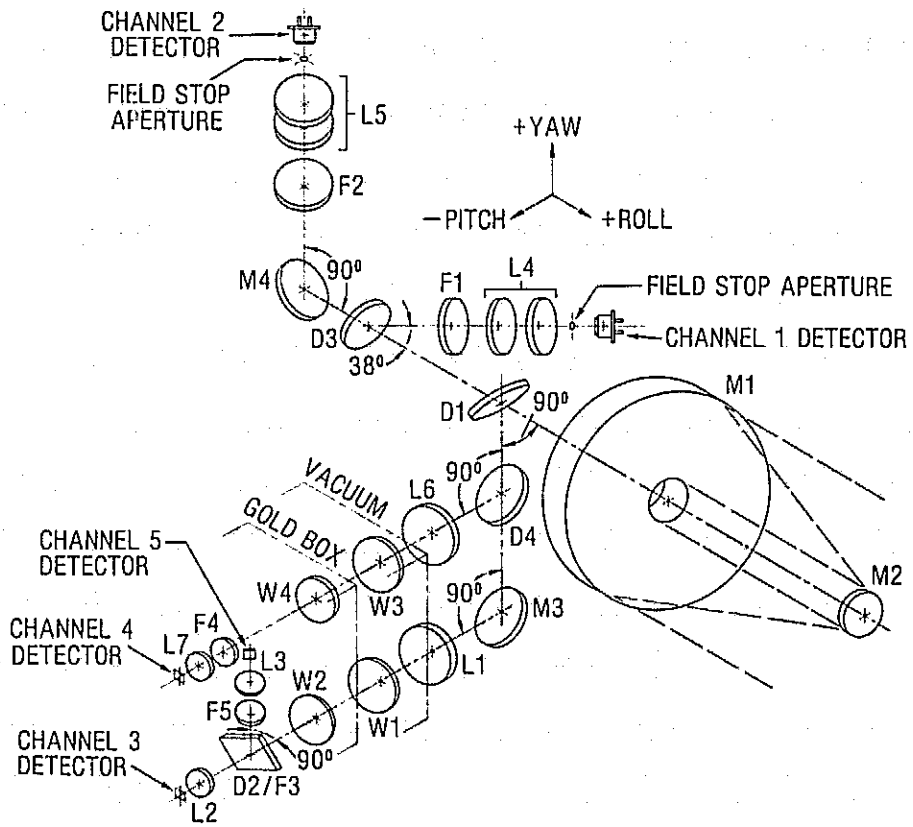

Figure 10. AVHRR/2 — Optical Elements

of biological oceanography. It differs from the AVHRR in that it is an experimental sensor and will therefore be used to develop new applications rather than as an operational data collector as is the case with the AVHRR.

A summary of the CZCS is given in the same format as was used with the AVHRR/2 in Table 6. A comparison of Tables 5 and 6 reveals many similarities between the CZCS and the AVHRR/2. Basically, however, the two sensors are quite different, the CZCS is predominately a visible energy detector using a grating spectrometer to spectrally delineate most of its channels whereas the AVHRR/2 has mainly infrared channels and uses interference filters to separate the channels. A unique feature of the CZCS design is the ability of the scan mirror to tilt ±350 mr. thereby shifting the scan lines fore or aft of the

Table 6

Summary
Coastal Zone Color Scanner
CZCS

MISSION PARAMETERS

ORBIT ALTITUDE	– 955 KM
ORBIT INCLINATION	– 99°
ORBIT PERIOD	– 103.5 MIN.
SURFACE SPEED	– 6.6 KM/SEC
SPACECRAFT	– NIMBUS-G
LAUNCH	– OCTOBER 1978

CZCS SYSTEM CHARACTERISTICS

GENERAL

6 CHANNEL SCANNING RADIOMETER, VIS AND IR CAPABILITY
PHYSICAL: 69 X 43 X 26 CM, 25.8 KG
ELECTRICAL: 24.3 WATTS AVG., < 40 WATTS PEAK
DATA OUTPUT: 8 BIT DIGITAL, 3.94×10^6 BITS/SEC (MAX), 8×10^5 BITS/SEC (AVG.)
MANUFACTURER: BALL BROTHERS RESEARCH CORP., BOULDER. COLO.

SCANNER

8.0 HZ, 80 POLE HYSTERESIS SYNCHRONOUS MOTOR
ELLIPTICAL BERYLLIUM SCAN MIRROR
±350 MR TILT IN PITCH IN 540 STEPS

ELECTRICAL

8 BIT A/D CONVERTER, SIMULTANEOUS SAMPLE AND HOLD
22 ANALOG TELEMETRY POINTS
30 DIGITAL TELEMETRY POINTS
38 COMMANDS

COOLER

2 STAGE PASSIVE RADIANT COOLER FOR 1 CHANNEL
113K DESIGN TEMP., 120K OPERATING TEMP.
COVER/EARTH SHIELD DEPLOYS OR CLOSES ON COMMAND
BENCH OPERABLE

OPTICS

17.8 CM DIAMETER CASSEGRAIN F/4 TELESCOPE

Table 6 (Cont'd)

WADSWORTH TYPE GRATING SPECTROMETER (CHAN. 1-5)
POLARIZATION SENSITIVITY < 1.5 PERCENT
0.865 MR IFOV, 0.83 X 0.83 KM FOOTPRINT
SPATIAL RESOLUTION (MTF) > 0.4 FOR 1 IFOV
CHANNELS REGISTERED WITHIN 0.15 MR ALL DIRECTIONS
SCANNING FIELD OF VIEW ±700 MR

PERFORMANCE

CHANNEL	SPECTRAL RANGE	DETECTOR TYPE	S/N	NETD
1	.433-.453 μm	Si	217	NA
2	.510-.530 μm	Si	218	NA
3	.540-.560 μm	Si	201	NA
4	.660-.680 μm	Si	114	NA
5	.700-.800 μm	Si	308	NA
6	10.5-12.5 μm	HgCdTe	303	0.2K (270K)

spacecraft nadir point. This is done in order to avoid the specular reflection of the sun from the water's surface commonly known as sun-glint. The amount and direction of this tilt is commandable from the ground.

A line drawing of the CZCS pointing out the major features is given in Figure 11, and a photograph of the scanner mounted on a laboratory test stand is shown in Figure 12. As discussed in Section III, the data rate of the CZCS is too large for a complete orbit's output to be stored using present tape recorders. Consequently, only a few minutes of data per orbit will be stored, using stored commands for preselection of target areas. The majority of the data will be obtained via direct transmissions while in view of ground stations. The location of these stations, however, does give extensive coverage of coastal areas in both North America and Europe.

Figure 13 is a diagram of the CZCS optical elements. A unique feature of this design is the pseudopolarizer consisting of two birefringent wedges that are located just prior to the concave 600 line/mm grating which is highly polorizing. Using these wedges and careful optical design, the polarization of the radiometer is kept at less than 2% for channels 1-4, thereby, preserving the radiometric accuracy of the sensor while viewing polorized scenes.

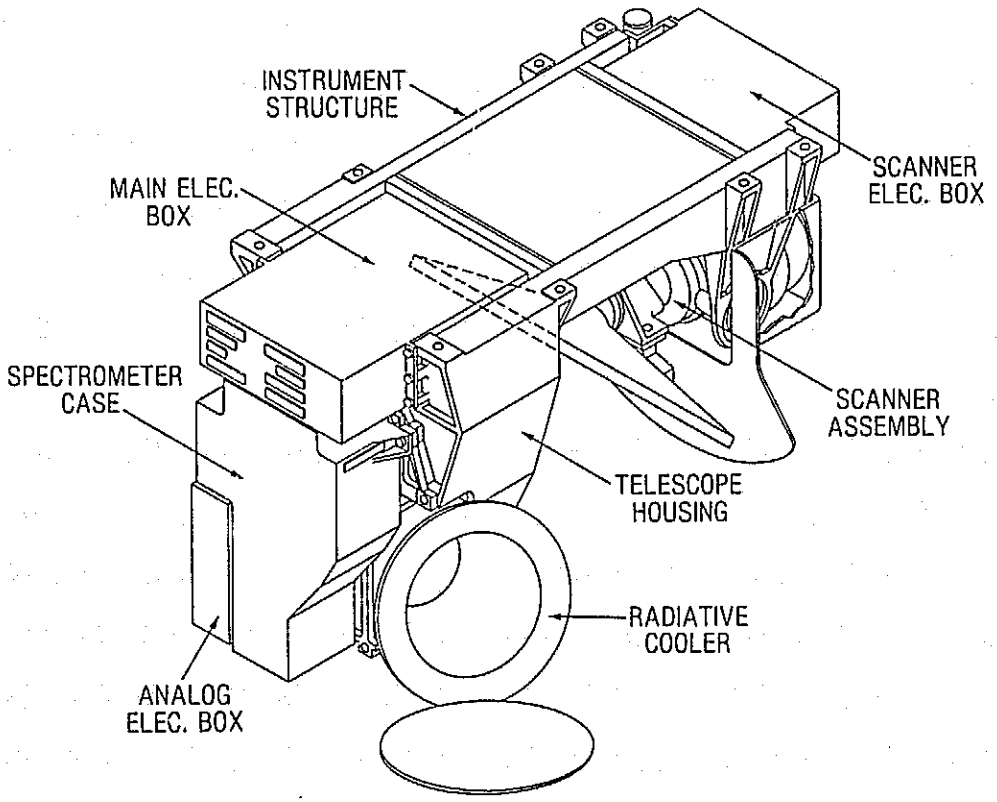

Figure 11. CZCS-Major Components

VIII. NEW TECHNOLOGY

The preceding sections have examined the present status of scanning radiometer system design and have presented several existing spacecraft and aircraft sensors as examples of implementation of these design practices. Although the example sensors have either been in use for only a brief time or are still being fabricated and tested, their designs were finalized some 1-3 years back and, consequently, do not include some of the latest innovations. Therefore, this section will briefly examine present trends in visible and infrared imaging radiometer design and developments in various types of system hardware. This discussion is not intended to be comprehensive but is meant to sketch out probable trends in the development of this type of sensor over the next few years. The reader is urged to examine the current literature for detailed descriptions of individual topics.

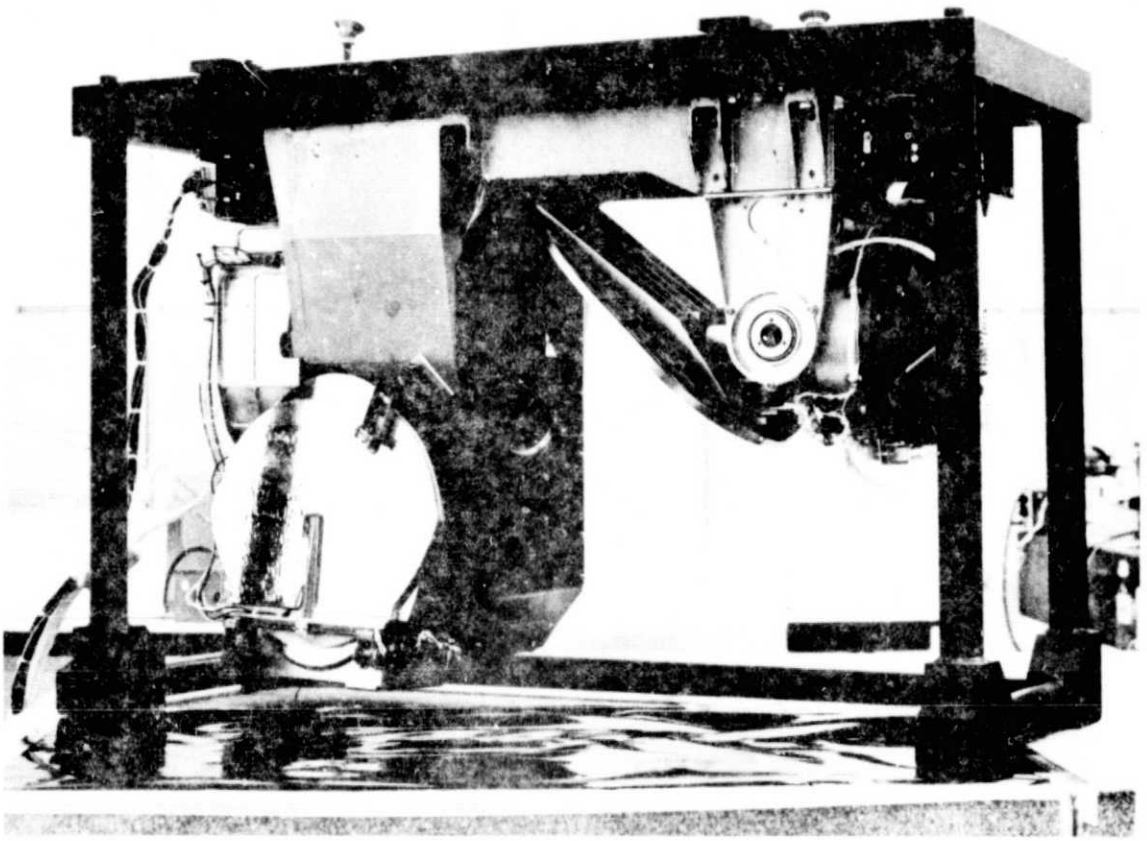

Figure 12. Nimbus-G CZCS

From the discussion of Section III, it is apparent that among the major difficulties of scanning radiometry are the brief dwell time on each IFOV and the inherent complexity of mechanical scanners. Both of these problems are being addressed through the development of large detector arrays. For example, a linear array of a few hundred to several thousand detector elements can be used to form a single scan line whose image is swept along the surface by the motion of the sensor platform. Consequently, the need for a scan mirror is eliminated and the dwell time on each IFOV is increased by the number of elements in the array divided by the efficiency of the mechanical scanner and, using equations (5) and (7), the signal-to-noise increases by the square root of this factor. This increase in signal-to-noise can be traded for increased spatial or spectral resolution if so desired. One and two dimensional arrays of silicon detectors with integrated CCD readouts have been available for some time. The so-called "pushbroom" scanners using linear silicon arrays have been proposed for spaceborne applications and are presently under construction (15) for airborne use. Unfortunately, the development of integrated infrared detector arrays has

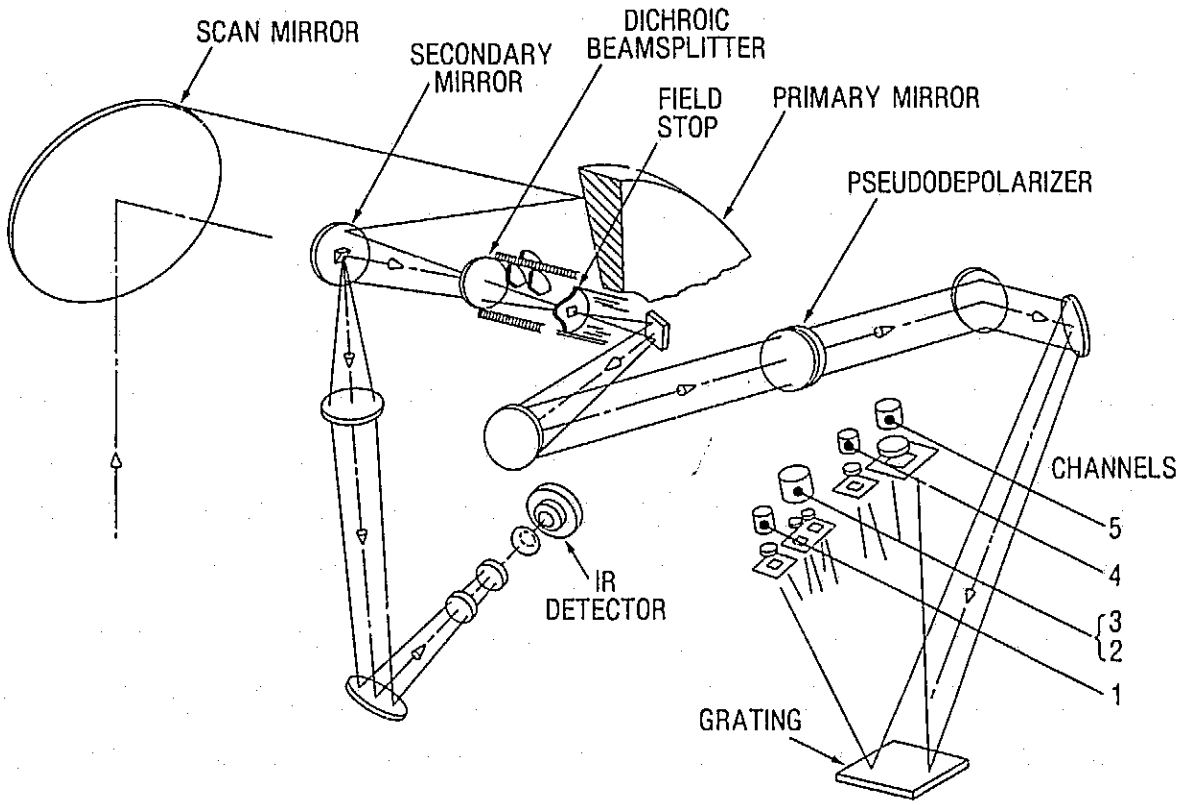

Figure 13. CZCS Optical Elements

proven to be a difficult task. The most promising results to date appear to be the hybrid arrays in which the multi-element detector chip and the integrated read-out electronics chip are hardwired together. This technology is available today but is rather cumbersome to implement for large numbers of detector elements.

The use of two-dimensional arrays can further increase the signal-to-noise and/or resolution of a radiometer. The usual mode of implementation for moving platforms is for the array to view a given scene on the surface for as long a period as necessary via image motion compensation. Preselected targets can be acquired by stored commands.

Another major problem of scanning radiometers, touched on briefly in the last part of Section III, is their enormous data output. For many applications, it is possible to reduce this flood of data by digital processing prior to transmission or storage. This processing can take the form of a simple averaging of several pixels as will be done with the AVHRR data or it may involve complex analysis. The means of carrying out this on-board processing can be a hardwired system or it can be a remotely programmable computer. The latter has the advantage

that changes in the performance of spacecraft sensors can be adjusted for by reprogramming after launch. Such systems exist today, and there will probably be a marked increase in their data processing capabilities over the next few years.

Problems in data storage and transmissions are being attacked on two fronts. Solid-state mass storage devices have undergone intense development with the aim of using them to replace the present tape recorders and they appear to be nearing this goal. In addition, synchronous satellite systems such as the Tracking and Data Relay Satellite System (TDRSS) are being developed so that data from aircraft or orbiting satellite sensors can be relayed directly to a ground station from any spot on the globe.

Due to increasingly sophisticated radiometry requirements, the development of large arrays of infrared detectors, and the need to locate spectral channels in the far infrared, there is an ever-increasing need for larger capacity, lower temperature cryogenic coolers. These will take the form of large passive coolers, large capacity LHe dewars, and high thermal capacity and/or low temperature closed-cycle systems.

Finally, one of the greatest impacts on sensor design technology will probably arise from the advent of the Shuttle/Spacelab era. Not only will this provide a large spaceborne platform with direct scientist/operator control for the development of new remote sensing techniques, but, due primarily to its low orbit, it will make possible combined passive, and active visible and infrared sensors through the use of laser ranging and radiometry.

REFERENCES

1. Reeves, R. G., Arson, A., and Landen, D., Editors, Manual of Remote Sensing, American Society of Photogrammetry, Falls Church, Va., 1975.

2. Lintz, I., and Simonett, D. S., Editors, Remote Sensing of the Environment, Addison Wesley, Reading, Mass., 1976.

3. Derr, V. E., Remote Sensing of the Troposphere, U.S. Dept. of Commerce, National Oceanic and Atmospheric Administration, Boulder, Colo., 1972.

4. Lloyd, J. M., Thermal Imaging Systems, Plenum Press, New York, N. Y., 1975.

5. Hudson, R. D., Infrared System Engineering, John Wiley and Sons, New York, N. Y., 1969.

6. McLean, J. T., "Operation Manual for 30-Inch Diameter Spherical Integrator Source for the AVHRR on TIROS-N," NASA/GSFC X-942-75-18, 1975.

7. Goldberg, I. L., "A Very High Resolution Radiometric Equipment for ATS-F and G," NASA/GSFC Preprint X-622-68-26, Greenbelt, Md., 1968.

8. Juarez, D., "Advanced Very High Resolution Radiometer, Mod 2, Technical Description," Contract #NAS5-23400, ITT Aerospace/ Optical Division, Ft. Wayne, Ind., 1976.

9. Richard, H. L., Technical Officer Nimbus-G/CZCS, personal communication.

10. Barnes, W. L., and Escoe, D., "Ocean Temperature Scanner Experiment Plan," NASA/GSFC Preprint X-941-77-94, Greenbelt, Md., 1977.

11. Prabhakara, C., Conrath, B. J., and Kunde, V. G., "Estimation of Sea Surface Temperature From Remote Sensing in the 11-13 μm Window Region," Journal Geophysical Research, Vol. 79, No. 33, Nov. 1974. pp. 5039-5044.

12. Blaine, L. R., Murphy, C. J., and Barnes, W. L., "Ocean Color Scanner Experiment," NASA/GSFC Preprint X-941-77-153, Greenbelt, Md., 1977.

13. Juarez, D., "Advanced Very High Resolution Radiometer Technical Description, Revision B," Contract #NAS5-21900, ITT Aerospace/ Optical Division, Ft. Wayne, Ind., 1974.

14. Donohue, M. J., AVHRR and AVHRR/2 Systems Engineer, personal communication.

15. Ostrow, H., NASA/GSFC, personal communication.